

MSC p43 required for axonal development in motor neurons

Xiaodong Zhu^{a,b}, Yang Liu^b, Yanqing Yin^b, Aiyun Shao^b, Bo Zhang^b, Sunghoon Kim^c, and Jiawei Zhou^{b,1}

^aLaboratory of Molecular Cell Biology, Institute of Biochemistry and Cell Biology, and ^bState Key Laboratory of Neuroscience Institute of Neuroscience, Shanghai Institutes for Biological Sciences, Chinese Academy of Sciences, Shanghai 200031, China; and ^cCenter for Medicinal Protein Network and Systems Biology, College of Pharmacy, Seoul National University, Seoul 151-742, Korea

Edited by Paul R. Schimmel, The Scripps Research Institute, La Jolla, CA, and approved July 28, 2009 (received for review March 4, 2009)

Neuron connectivity and correct neural function largely depend on axonal integrity. Neurofilaments (NFs) constitute the main cytoskeletal network maintaining the structural integrity of neurons and exhibit dynamic changes during axonal and dendritic growth. However, the mechanisms underlying axonal development and maintenance remain poorly understood. Here, we identify that multisynthetase complex p43 (MSC p43) is essential for NF assembly and axon maintenance. The MSC p43 protein was predominantly expressed in central neurons and interacted with NF light subunit *in vivo*. Mice lacking MSC p43 exhibited axon degeneration in motor neurons, defective neuromuscular junctions, muscular atrophy, and motor dysfunction. Furthermore, MSC p43 depletion in mice caused disorganization of the axonal NF network. Mechanistically, MSC p43 is required for maintaining normal phosphorylation levels of NFs. Thus, MSC p43 is indispensable in maintaining axonal integrity. Its dysfunction may underlie the NF disorganization and axon degeneration associated with motor neuron degenerative diseases.

assembly | axon degeneration | multisynthetase complex | neurofilament

The development and maintenance of neuronal axons are essential for the establishment of neuron connectivity and for correct neural function. Neurofilaments (NFs), a subtype of intermediate filaments (IFs), form part of the cytoskeleton that confers the intracellular scaffold and mechanical stability of neurons (1, 2). They are dynamic structures known to play key roles in neuronal development and function, such as neuronal morphogenesis, neuronal migration, axonal growth, synaptic plasticity, and intracellular transport (3). Five major types of IF proteins are expressed in adult neurons: 3 neurofilament proteins [neurofilament-light subunit (NF-L), neurofilament-medium subunit (NF-M), and neurofilament-heavy subunit (NF-H)], peripherin, and α -internexin (3). Studies with either gene targeting or a transgenic approach provide evidence that deficiency of NF proteins and disorganization of the neuronal NF network can result in abnormalities in the motor axon caliber, defective axonal transport, axon atrophy and loss, and motor dysfunction (3). Despite the abundance and crucial role of NFs in neurons, the molecular basis for the development and maintenance of neuronal axons is not fully understood.

Posttranslational modifications and binding partners are keys for regulation of the dynamics and functions of NFs. Phosphorylation takes center stage for their regulation (4). Phosphorylation of NFs is slow and orchestrated by a range of enzymes, and NFs have been reported to be substrates of many kinases (5). The phosphorylation of NFs plays a key role in NF assembly and turnover; in forming cross-bridges between NFs, actin filaments, and microtubules (MTs); in axonal transport of NFs themselves; and in promoting NF integration into the cytoskeleton underlying dendrite arborization and axonal caliber determination and stability (4, 6, 7). Studies with transgenic mice overexpressing NF proteins with phosphorylation-mimicking mutations show that NF hyperphosphorylation results in disorganization of the NF network, leading to NF inclusions, defective axonal transport,

and axon degeneration (8–13). Moreover, the abnormal accumulation of hyperphosphorylated NFs is a pathological hallmark of many human neurodegenerative disorders, including ALS, dementia with Lewy bodies, Parkinson's disease, and neuropathies (14–16). Thus, NF hyperphosphorylation is involved in the pathogenesis of neurodegenerative disorders. Phosphorylation and dephosphorylation of NF proteins are complex processes that occur predominantly within the axon on different phosphate acceptor sites in the NF subunit (4, 6). However, the mechanism regulating NF phosphorylation remains elusive.

In the present study, we found that multisynthetase complex (MSC) p43 [also called aminoacyl-tRNA synthetase (ARS)-interacting multifunctional protein 1], a cofactor of the macromolecular ARS complex, was predominantly expressed in central nervous system (CNS) neurons and interacted with NF-L. The direct binding between MSC p43 and NF-L was further confirmed using coimmunoprecipitation and the fluorescence resonance energy transfer (FRET) method. Either overexpression or depletion of MSC p43 altered the phosphorylation level of NFs and resulted in disassembly of the NF network, suggesting that NF phosphorylation is normally regulated at an optimal level. In MSC p43-deficient mice, motor neurons exhibited axon degeneration, along with resultant defects of neuromuscular junctions (NMJs), muscular atrophy, and motor dysfunction. Taken together, our results demonstrate that MSC p43 has a previously undescribed function as an essential regulator of NF assembly.

Results

Characterization of MSC p43 Expression in the CNS. The expression and localization of MSC p43, although well characterized in other systems (17), are entirely unknown in the CNS. Using either immunohistochemistry or *in situ* hybridization, we found that MSC p43 was expressed in the neurons of a variety of CNS regions, including the ventral horn of the spinal cord and the hippocampus [supporting information (SI) Fig. S1].

Muscle Atrophy and NMJ Defects in MSC p43-Null Mice. To unravel the potential biological function of MSC p43 in the CNS, we examined the behaviors of MSC p43-deficient mice (18, 19). Most MSC p43-null mice displayed weight loss, decreased fertility and grooming, and spontaneous and sometimes spastic tremors, although the severity and onset of the symptoms (about 1 month after birth) were variable among littermates. Most of

Author contributions: J.Z. designed research; X.Z., Y.L., Y.Y., A.S., and B.Z. performed research; S.K. contributed new reagents/analytic tools; X.Z., S.K., and J.Z. analyzed data; and J.Z. wrote the paper.

The authors declare no conflict of interest.

This article is a PNAS Direct Submission.

Data deposition: The sequence reported in this paper has been deposited in the GenBank database (accession no. U10118).

¹To whom correspondence should be addressed. E-mail: jwzhou@ion.ac.cn.

This article contains supporting information online at www.pnas.org/cgi/content/full/0901872106/DCSupplemental.

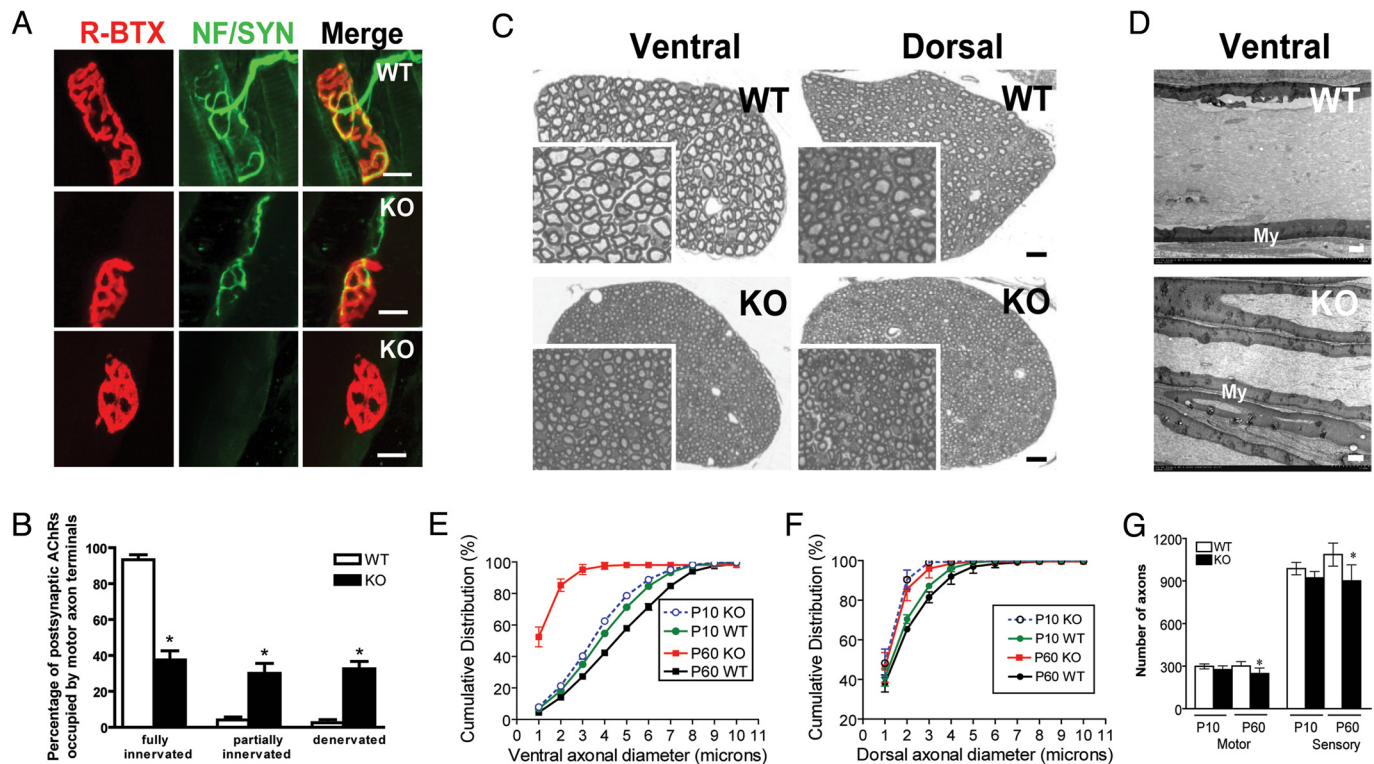


Fig. 1. NMJ and motor axon degeneration in MSC p43-null mice. (A) NMJs in the gastrocnemius muscle of 2-month-old WT and age-matched MSC p43-null mice. The motor nerve terminal (green) and the AChRs on the muscle (red) are shown. (Scale bars: 20 μm .) (B) Quantification of the NMJs in gastrocnemius muscles ($n = 6$ MSC p43 mutants and 6 littermate control mice, 100 NMJs in gastrocnemius muscles examined per mouse). Values are mean \pm SEM (2-way ANOVA with post hoc test). A significant difference between the 2 groups was marked as * $P < 0.05$. (C) Axonal morphology in ventral and dorsal roots from P60 WT and MSC p43-null mice by light microscopy of toluidine blue-stained cross semithin sections. Inserts show transverse sections of whole roots at higher magnifications. (Scale bars: 100 μm .) (D) EM ultrastructural analysis of large myelinated axons from WT and MSC p43-null ventral roots at P60 are shown. My, myelin sheath. (Scale bars: 400 nm.) (E and F) Axonal areas and calibers were determined, using the Stereo Investigator and NeuroLucida software programs (MBF Bioscience), by randomly sampling at least 300 myelinated axons in each root and at least 3 roots of each sample from 6 mutants or 6 littermate control mice. Values depict mean \pm SEM. A significant difference between the 2 groups (P60 WT and P60 KO mice) is evident (nonparametric ANOVA; $P < 0.01$, Kolmogorov–Smirnov test). (G) Myelinated axons are counted in the ventral and the dorsal roots of control and mutant animals at P10 and P60 ($n = 6$ of each genotype). The values in G are the mean of the axon number in each root \pm SEM (t test, * $P < 0.05$).

these mice could not extend their hind limbs when suspended by the tail (Fig. S2A) and showed lameness of the hind limbs (Movies S1 and S2). Many MSC p43-null mice exhibited slower gaits and decreased motor activity, as shown by the Rotarod assay (Columbus Instruments) (Fig. S2B).

Further histological studies showed that dysfunctions of motor behaviors noted previously were associated with widespread muscle atrophy. In 2-month-old MSC p43-null mice, there was pronounced atrophy of the large gastrocnemius muscle of the hind limb (Fig. S2C), including the reduction of muscle fiber density (Fig. S2C and D), muscle atrophy and fibrosis (Fig. S2C), and clustering of muscle fibers (Fig. S2C). The density of muscle fibers decreased markedly to a level $\approx 44\%$ of that in the normal mice of the same age (Fig. S2D).

Next, we examined the NMJs of MSC p43-deficient mice at developmental and adult stages, including embryonic day (E) 18 and postnatal day (P) 5, P15, and P60 (2 months old). The NMJs in MSC p43-null mutants were morphologically indistinguishable from those of WT mice at E18, P5, and P15 (Fig. S3A and B). In 2-month-old WT mice, NMJs in gastrocnemius muscles were well developed. Each muscle fiber in gastrocnemius muscles is contacted by branches of a single motor axon. The nerve terminals completely overlapped the postsynaptic AChR plaques on the muscle, as revealed by staining with tetramethylrhodamine-conjugated α -bungarotoxin (Fig. 1A and Fig. S3C). In P60 MSC p43-null mice, however, many muscle fibers exhibited partial or no innervation, with AChR plaques partially

covered by or completely devoid of the nerve terminal (Fig. 1A and Fig. S3D). Moreover, AChR plaques from MSC p43-null mice did not exhibit the normal “pretzel-like” morphology and, instead, had reduced complexity, apparent atrophy, and structure collapse (Fig. 1A and Fig. S3C and D).

The percentage of postsynaptic AChR plaques occupied by motor axon terminals was measured for 6 MSC p43 mutants and 6 littermate control mice (Fig. 1B). The control mice showed nearly full occupancy ($93.3 \pm 2.8\%$), whereas mutant mice showed that a substantial fraction of postsynaptic AChR plaques on muscle fibers was partially occupied ($30.0 \pm 5.6\%$) or fully denervated ($32.5 \pm 4.2\%$). Thus, the absence of MSC p43 results in severe atrophy in hind limb muscle and degeneration of motor nerve terminals, along with defective NMJs, consistent with hind limb weakness and abnormal motor functions.

Motor Axon Degeneration in MSC p43-Null Mice. The hind limb weakness and altered muscle morphology in MSC p43-null mice suggest degeneration of motor axons innervating the hind limb muscles. We initially examined the motor axons at P10 and found that the axons from control and mutant animals were indistinguishable by histological staining and EM ultrastructural analysis (Fig. S4A and B). Importantly, the largest myelinated axons of the MSC p43-null roots showed a mild decrease in size compared with the largest axons of control roots (Fig. 1E). However, the myelinated axons of the lumbar ventral roots in 2-month-old MSC p43-null mice, as shown in Fig. 1C, indeed exhibited an

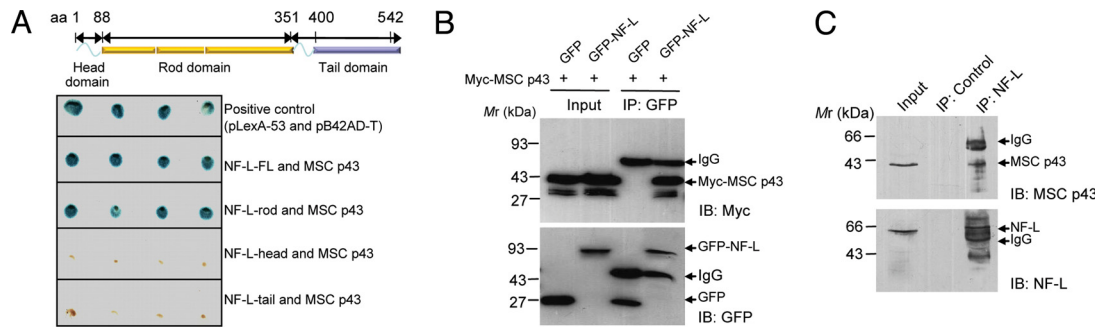


Fig. 2. MSC p43 binds NF-L directly. (A) Definition of the interaction domains of NF-L and MSC p43 by the yeast 2-hybrid expression system. A schematic representation illustrates the simplified primary structures of NF-L protein. The pLexA-53 and pB42AD-T serve as positive controls. (B) Immunoprecipitation (IP) and immunoblot (IB) analyses of cell lysates from HEK293T cells coexpressing GFP-NF-L and Myc-MS-C p43. (C) Coimmunoprecipitation of MSC p43 with NF-L proteins from mouse brain lysates; GFP antibody is used as a negative control in IP.

irregular shape and appeared shrunken and collapsed, with expanded intercellular space, and the axon diameter profile significantly shifted toward a smaller diameter as compared with that in WT mice (Fig. 1E). This reduction of the axon diameter was further confirmed by EM ultrastructural analysis, which also revealed apparently normal axon myelination in MSC p43-null mice (Fig. 1D). Histological analysis of the lumbar dorsal root also revealed a smaller but significant axon abnormality (Fig. 1F).

Moreover, we counted the number of axons in the motor and sensory roots. A significant reduction in myelinated axon number was observed in both the motor and sensory roots of 2-month-old MSC p43-null mice compared with control roots (Fig. 1G). However, such reduction was not found in WT and MSC p43-null mice at P10. These findings on motor axon progressive degeneration (axon atrophy and loss) attributable to MSC p43 depletion are consistent with the observed muscle atrophy and NMJ defects (Fig. 1, Fig. S2, and Fig. S3). To determine further whether motor axon atrophy and loss are attributable to motor neuron loss, we examined histological sections of the anterior horn of the lumbar spinal cord of the 2-month-old MSC p43-null mice. Both Nissl staining and NF immunostaining revealed no evidence of neuronal loss in the anterior horn (Fig. S4), although the white matter in the spinal cord showed some shrinkage (Fig. S4C). Together, these results suggest that MSC p43 depletion specifically impairs development of axon and innervated muscles.

MSC p43 Interacts Directly with NF-L. Given the remarkable motor neuropathy observed in ventral roots of MSC p43-deficient mice and the observation that MSC p43 colocalizes with NF-L (Fig. S1C), a critical component of cytoskeleton of motor neuron axons (1, 2), we hypothesized that MSC p43 contributes to axonal maintenance via interaction with NF-L. To test this hypothesis, we initially used the yeast 2-hybrid assay to examine whether MSC p43 physically interacts with NF-L and to map the interaction domain on NF-L. The β -galactosidase assay showed that both full-length (FL; amino acids 1–542) and the rod domain of NF-L (amino acids 89–400, containing 2 coiled-coil subdomains) interacted with MSC p43. In contrast, neither the NF-L-head (amino acids 1–88) nor NF-L-tail (amino acids 351–542) domain interacted with MSC p43 (Fig. 2A). Thus, the NF-L rod domain is sufficient for direct and specific interaction with MSC p43. Coimmunoprecipitation experiments further confirmed the NF-L interaction with MSC p43. MSC p43 was specifically coimmunoprecipitated with NF-L in cell lysates obtained from HEK 293T cells coexpressing Myc epitope-tagged MSC p43 (Myc-MS-C p43) and GFP epitope-tagged NF-L (Fig. 2B and Fig. S5A). Similarly, coimmunoprecipitation of endogenous proteins in adult mouse brain lysates was found using the

NF-L antibody (Fig. 2C), an effect not found in brain lysates of MSC p43-null mice (Fig. S5B).

The interaction between MSC p43 and NF-L was further examined in SH-SY5Y neuroblastoma cells using FRET. When YFP-tagged MSC p43 and CFP-tagged NF-L were coexpressed in these cells (Fig. S5D), we observed significant FRET between YFP-MS-C p43 and CFP-NF-L, indicating their close contact with each other (Fig. S5C and E). Measurements of FRET efficiency showed that proximity between MSC p43 and NF-L was comparable to that between CFP and YFP on the fusion protein CFP-15Aa-YFP (Fig. S5E), consistent with the colocalization of endogenous MSC p43 and NF-L in spinal motor neurons (Fig. S1C). However, MSC p43 did not assemble with filamentous GFP-NF heteropolymers (Fig. S6). Taken together, these results demonstrate that MSC p43 specifically interacts with NF-L both in vitro and in vivo.

MSC p43 Dysregulation Causes NF Network Disorganization. Because NF-L is a key subunit for NF assembly (20), we investigated the consequence of MSC p43 overexpression on the formation of an NF network in SH-SY5Y neuroblastoma cells, using GFP-NF as a marker for NF assembly. We found that in most GFP-NF and Myc-MS-C p43 double-transfected cells, GFP-NF accumulated in the cell body and neuronal processes in the form of punctuated aggregates characteristic of disrupted NF assembly. In contrast, filamentous GFP-NF was found to distribute uniformly throughout the cells when GFP-NF plasmid was cotransfected with the control Myc plasmid (Fig. S7A). Counting of cells exhibiting punctuated or filamentous distribution of GFP-NFs showed that high-level exogenous MSC p43 caused disassembly of all NFs (Fig. S7B). Furthermore, the extent of disassembly of NFs, as shown by the fraction of soma area covered by filamentous NF-GFP, increased monotonically with the level of Myc-MS-C p43 expression (Fig. 3A and B). These results indicate that MSC p43 inhibits the formation of NFs in a dose-dependent manner. In contrast to that for NF assembly, MSC p43 overexpression had no effect on the formation of actin filaments, MTs, and vimentin IFs (Fig. S7C). Thus, MSC p43 inhibits the formation of NFs specifically. The role of MSC p43 in NF polymerization was also tested in a human adrenal-carcinoma-derived cell line (SW13 vimentin-negative cells) deficient in endogenous IFs (20). We found that cotransfection of GFP-NF and MSC p43 plasmids resulted in similar NF disruption as in SH-SY5Y cells (Fig. S8).

Along with MTs and microfilaments, NFs constitute the cytoskeleton that stabilizes the axon (3). Given that MSC p43 depletion caused markedly progressive degeneration of ventral root axons (Fig. 1), we further examined axonal ultrastructure using EM. The cytoskeleton network in MSC p43-null axons at P10 was indistinguishable from that of control (Fig. S9), whereas,

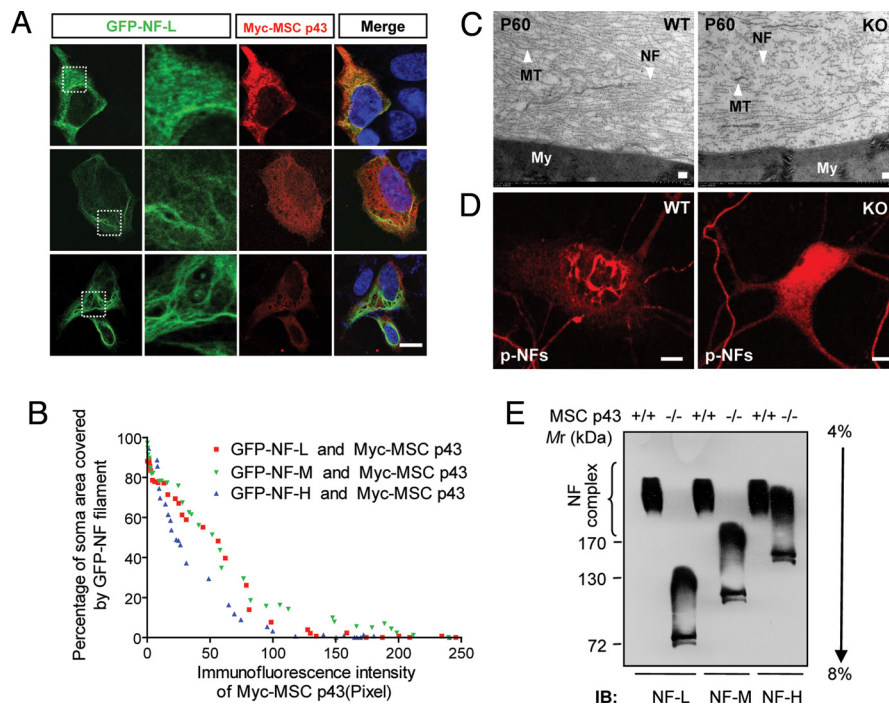


Fig. 3. MSC p43 dysregulation causes NF network disorganization. (A) SH-SY5Y cells were transfected with Myc-MSC p43 and one of the GFP-NFs. In the same visual field, according to immunofluorescence intensity using anti-Myc antibody, Myc-MSC p43 expression is scored as higher (*Top*), intermediate (*Middle*), and lower (*Bottom*) levels. (Scale bar: 10 μ m.) (B) Quantitative data as shown in A. The NF area per cell and the total area of the corresponding cell are determined using the Stereo Investigator and NeuroLucida software programs (MBF Bioscience) as described in *SI Text*. Cells in the same visual field (NF-L, $n = 31$; NF-M, $n = 33$; and NF-H, $n = 31$) are randomly scored. (C) Ventral roots of lumbar spinal cord are isolated from MSC p43-null and WT mice and processed directly for transmission EM. Portions of large myelinated axons from WT and MSC p43-null ventral roots are shown. My, myelin sheath. (Scale bars: 100 nm.) (D) NF network in primary cultured hippocampal neurons from WT and MSC p43-null mice was revealed using phospho-NF-M/H antibodies. (Scale bars: 5 μ m.) (E) Gel shift assay was used to show the association among the 3 NF subunits.

unlike the dense and well-aligned NFs and MTs in WT motor axons, NFs and MTs were disorganized in motor axons of MSC p43-null mice at P60, with shorter, fewer, and disordered NFs (Fig. 3C). In primary cultured hippocampal neurons of MSC p43-null mice, diffused dot-like NF proteins were observed, in contrast to the NF-like structure seen in WT mice (Fig. 3D). A gel shift assay further showed that in WT axons, NF triplet subunits (NF-L, NF-M, and NF-H) appeared to be obligate heteropolymers (high-molecular-weight NF complex), whereas in MSC p43-null axons, these subunits existed as disassociated monomer and the NF complex collapsed or disappeared altogether (Fig. 3E). These data support the notion that MSC p43 dysregulation results in NF disassembly in motor axons, which may contribute to axon degeneration.

MSC p43 Is a Negative Regulator of NF Phosphorylation. Phosphorylation of NF proteins is known to regulate NF organization and function (21, 22). To investigate whether MSC p43 regulates NF assembly by affecting phosphorylation of the NF proteins, we examined NF protein phosphorylation in hippocampal neuronal cultures. Interestingly, overexpression of GFP-MSC p43 in these cells resulted in a marked reduction in the level of phosphorylated NF proteins, as shown by the intensity of immunofluorescence staining of phosphorylated NF proteins in the neurites compared with that found in control cells expressing GFP (Fig. 4A and B). In contrast, MSC p43 depletion caused a notable increase (2.49-fold) in the level of phosphorylated NF proteins in the neurites compared with that in WT neurons (Fig. 4C). The effect of MSC p43 on down-regulating NF protein phosphorylation was further examined by Western blot analysis. We found that hippocampal neurons transfected with GFP-MSC p43 showed a marked reduction in levels of phosphorylation for

NF-M and NF-H (about 40% and 50% reduction, respectively) compared with that of the GFP control (Fig. 4D and G). Conversely, MSC p43 depletion caused a dramatic increase in levels of phosphorylation for NF-M and NF-H in cultured hippocampal neurons (Fig. 4E and H). Moreover, the levels of phosphorylation for NF-M and NF-H in the spinal cord of MSC p43-null mice were elevated by 2- and 3-fold, respectively, compared with that found in WT littermates (Fig. 4F and I). In contrast, the total level of NF-H, NF-M, and NF-L, as indicated by antibodies against the nonphosphorylated site of the NF proteins, showed no significant change (Fig. 4F and J). Taken together, these results showed that MSC p43 is a negative regulator of NF phosphorylation.

Discussion

There is accumulating evidence for the multiple functions of MSC p43, including extracellular function as a cytokine for monocytes, endothelial cells, and fibroblasts and as a glucagon-like hormone (23) and intracellular function in activating immune dendritic cells (19). However, the role of MSC p43 in the adult CNS has not been investigated. Moreover, the mechanisms of regulating the assembly of NF subunits into filaments have not been fully understood. In the present study, we show that MSC p43 is expressed in neurons of the brain and spinal cord. It directly associates with NF-L and modulates NF protein phosphorylation and assembly of NFs. By influencing NF network assembly, MSC p43 may regulate axon development and maintenance, representing a distinct function in the CNS.

MSC p43 Is a Previously Undescribed Negative Regulator of NF Phosphorylation. Both increases and decreases in the phosphorylation of NF proteins modulate the formation of the NF

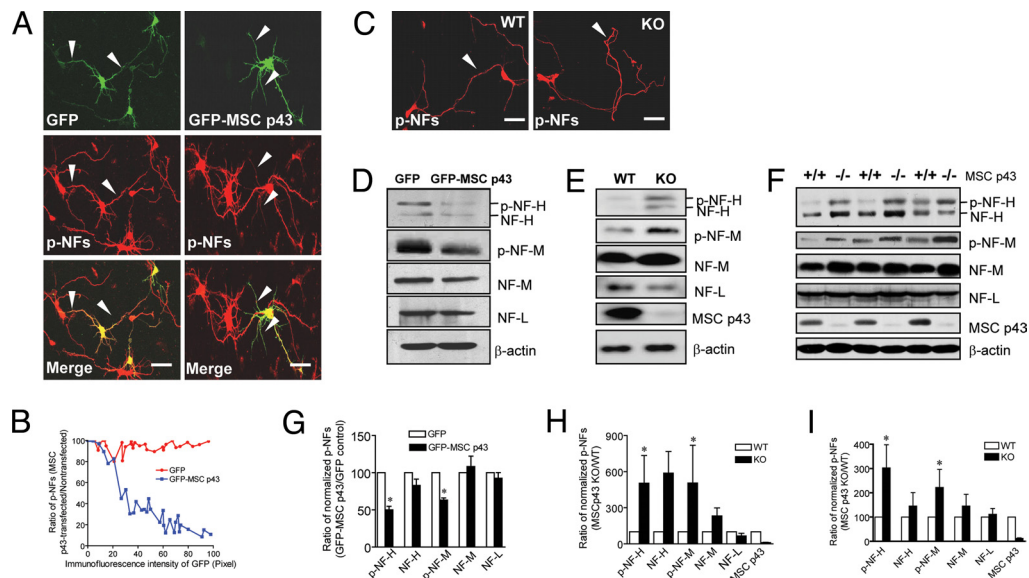


Fig. 4. MSC p43 is a negative regulator of NF phosphorylation. (A) Cultured hippocampal neurons from WT mice were transfected with GFP-MSC p43 or GFP, followed by immunostaining using antibodies against phospho-NF-M/H. Arrowheads indicate neurites. (B) Average immunofluorescence intensity of GFP and p-NFs in cells is quantitated by using Image Pro-Plus software (Media Cybernetics). In the same field, the ratio of the average immunofluorescence intensity of p-NFs in neurites of transfected neurons and that in neurites of nontransfected neurons were determined. The curve displays the ratio and the average immunofluorescence intensity of GFP ($n = 31$ each). (C) Cultured hippocampal neurons from WT and MSC p43 KO mice were stained with antibodies against phospho-NF-M/H. Arrows indicate neurites. (Scale bar: 10 μm .) (D) Western blot analysis of cell lysates from cultured hippocampal neurons electroporated with GFP-MSC p43 or GFP control. (E) Western blot analysis of cell lysates from cultured hippocampal neurons of MSC p43-null and control mice. (F) Expression levels of NF proteins in the spinal cord of mice were analyzed by Western blot. (G and H) Quantification of the data shown in D and E, respectively. (I) Quantitative data as shown in F ($n = 7$ each). β -actin serves as a protein-loading control. Experiments were performed at least 3 times. Values in G, H, and I are mean \pm SEM (t test, $*P < 0.05$), compared with GFP control or WT mice, respectively.

network by altering the assembly dynamics involving interactions among NF subunits or their interactions with other proteins (24), including many kinases. The present study has identified MSC p43 as a nonkinase protein capable of regulating NF phosphorylation. Our evidence shows that overexpression of MSC p43 led to a decreased level of NF protein phosphorylation and NF collapse in SW13 vimentin-negative cells and primary cultured neurons, whereas MSC p43 depletion caused hyperphosphorylation of NF proteins and NF network disassembly in primary cultured neurons and motor axons, resulting in phenotypes similar to those observed in mice lacking the NF-L gene (25). On the basis of these observations, we propose that MSC p43 tightly regulates NF assembly via interaction with NF-L monomer at the rod domain, an interaction that prevents the phosphorylation of NF proteins. Thus, depletion of MSC p43 from NF-L may expose the NF-L rod domain in a conformation that exposes NFs to undergo hyperphosphorylation, whereas excess binding of MSC p43 to NF-L may enhance polymeric rod-rod interaction and change the conformation to one that inhibits NF phosphorylation.

Given that MSC p43 is critical for regulation of NF phosphorylation, alteration of MSC p43 levels may disturb the homeostasis of NF protein phosphorylation, causing NF network collapse. Interestingly, this MSC p43 action is similar to that of NUDEL, another protein binding directly to the rod domain of NF-L. Down-regulation of NUDEL by siRNA promoted NF-H phosphorylation and prevented NF assembly (26), suggesting critical roles of NF rod domain-binding protein for regulation of NF phosphorylation levels. This is consistent with the notion that an optimal level of NF phosphorylation is required for NF assembly. Interestingly, neither MSC p43 nor NUDEL is assembled into filamentous NF heteropolymers. However, unlike NUDEL, which facilitates *in vitro* polymerization of NFs (26), MSC p43 inhibits NF polymerization. Thus, it is likely that MSC p43 works together with NUDEL to coordinate NF polymerization.

NF protein phosphorylation is known to be regulated by many kinases (mitogen-activated protein kinase, glycogen synthase kinase-3 β , ERK, cyclin-dependent kinase 5, protein kinase A/C, phosphatases, and NF-associated protein) (5–7), indicating that NFs are targeted and modulated by multiple neuronal signaling cascades. MSC p43 has been found to be the key regulator of many kinases *in vivo*. As an extracellular cytokine, MSC p43 activates JNK and ERK in immune and endothelial cells (23). Moreover, previous evidence has shown that MSC p43 is a key suppressor of protein phosphorylation in intracellular signaling cascades. Phosphorylation of TGF- β signal mediators, Smad2 and Smad3, is enhanced by the deletion or knockdown of MSC p43 (23). Thus, hyperphosphorylation of NFs in MSC p43-null mutants could result from activation of certain kinases that are otherwise suppressed by MSC p43 under physiological conditions.

Potential Role of MSC p43 in the Pathogenesis of Charcot-Marie-Tooth Neuropathy Type 2D. Charcot-Marie-Tooth (CMT) neuropathies are inherited disorders of the peripheral nervous system. A specific form of the disease, CMT neuropathy type 2D, has been associated with dominant point mutations in the gene GARS, encoding glycyl-tRNA synthetase (GlyRS) or tyrosyl-tRNA synthetase (TyrRS) (27–29). Intriguingly, MSC p43-null mice show very high phenotypic similarities with CMT neuropathy type 2D, including large-diameter axon loss from both motor and sensory peripheral nerves, distal motor neuropathy with impairment in synaptic connectivity at NMJs, and muscle denervation in the hind limb (30).

ARS complexes contain TyrRS and GlyRS, which potentially interact with MSC p43 (23). Moreover, several mutations in the NF-L rod domain have been reported in CMT neuropathy type 2D (28, 31). These findings suggest that MSC p43 may be a potential molecular linker between components of the protein biosynthesis machinery (ARs) and NFs in CMT neuropathy

type 2D. The exact role of MSC p43 in the pathogenesis of CMT neuropathy type 2D is to be investigated in future studies.

Materials and Methods

Antibodies and Constructs. The antibodies and constructs used are described in *SI Text*. The rabbit anti-MSA p43 antibody was a kind gift from Dr. M. Clauss (Max Planck Institute for Physiological and Clinical Research, Bad Nauheim, Germany) (32). The specificity of MSC p43 antibody was confirmed by using immunoblot and immunohistochemical analyses (Fig. S1 A and F).

Protein Interaction Assays. The yeast 2-hybrid system was used to test whether there was interaction between MSC p43 and NF-L, as described previously (26). To detect direct interaction between 2 proteins in cells further, FRET measurements and coimmunoprecipitation were performed essentially as described (33). A gel shift assay was used to show whether NF subunits (NF-L, NF-M, and NF-H) were associated with each other in the NF complex as described previously (34). Details are given in *SI Text*.

Cell Culture, Transfection, and Immunostaining. All cell lines (SH-SY5Y, SW13 vimentin-negative, and HEK 293T) used in the present study were grown in DMEM/F12 (Invitrogen) containing 10% (vol/vol) FBS. Transient transfection of these cell lines was carried out with calcium phosphate or Lipofectamine 2000 (Invitrogen). The primary hippocampal neuronal culture was prepared according to the procedure described previously, with some modifications (35). Dissociated neurons were transfected using a Nucleofector device (Amaxa) and were cultured in Neurobasal medium supplemented with B27 (Invitrogen). Cells were fixed with 4% (w/vol) paraformaldehyde in PBS for 10 min and then immunostained using appropriate antibodies for the procedure (36).

Immunofluorescence, Confocal Microscopy, and Image Analysis. Sections were incubated with one primary antibody followed by incubation with a secondary antibody conjugated with either TRITC or FITC. The same sections were then incubated with another primary antibody, followed by incubation with the appropriate secondary antibody. For immunofluorescence of NMJs, muscle cryostat sections were mounted on slides and stained to visualize *en face* junctions (30). Cocktails of the following primary antibodies were used to visualize motor neuron nerves: mouse anti-NF (Sigma) and rabbit antisynaptophysin (Zymed). FITC-conjugated antirabbit and antimouse secondary antibodies were used. Tetramethylrhodamine-conjugated α -bungarotoxin (Molecular Probes) was used to visualize AChRs on the muscle cell surface. Sections were imaged using either a cooled CCD SPOT II (Diagnostic Instruments) on a microscope (BX51; Olympus) or a laser confocal microscope (Leica). Data were obtained and processed using Adobe Photoshop 7.0 software (Adobe Systems).

Statistical Analysis. The control group was compared with the different sample groups using either 1-way or 2-way ANOVA, followed by the *t* test. In some cases, a nonparametric Kolmogorov–Smirnov test was also used. Differences were considered significant when *P* values were <0.05.

ACKNOWLEDGMENTS. We thank Dr. M.M. Poo for discussion and editing of the manuscript; Dr. Q. Hu and Ms. W. Bian for technical support in confocal microscopy and data analysis; Drs. J.Y. Chen and M. Jiang for help in the Y2H assay; Dr. J.G. Chen for providing SW13 cell lines; Dr. C. Miller for providing NF-L, NF-M, and NF-H cDNAs; Dr. M. Clauss for providing MSC p43 antibodies; Dr. E.S. Sztlut for providing the plasmid GFP-250; and Drs. Z.G. Luo and F. Chen for NMJ analysis. This work was supported by grants from the Chinese Academy of Sciences, Chinese Ministry of Science and Technology (2006AA02Z184), Shanghai Metropolitan Fund for Research and Development (07DJ14005), Natural Science Foundation of China (30525041, 30623003, and 30621130075), State Key Program for Basic Research of China (2006CB500704), Acceleration Research of KOSEF (370C-20090015), and the 21st Frontier Functional Proteomics Research (370C-20090055).

- Herrmann H, Bar H, Kreplak L, Strelkov SV, Aebi U (2007) Intermediate filaments: From cell architecture to nanomechanics. *Nat Rev Mol Cell Biol* 8:562–573.
- Fuchs E, Cleveland DW (1998) A structural scaffolding of intermediate filaments in health and disease. *Science* 279:514–519.
- Lariviere RC, Julien JP (2004) Functions of intermediate filaments in neuronal development and disease. *J Neurobiol* 58:131–148.
- Sihag RK, Inagaki M, Yamaguchi T, Shea TB, Pant HC (2007) Role of phosphorylation on the structural dynamics and function of types III and IV intermediate filaments. *Exp Cell Res* 313:2098–2109.
- Petzold A (2005) Neurofilament phosphoforms: Surrogate markers for axonal injury, degeneration and loss. *J Neurol Sci* 233:183–198.
- Omary MB, Ku NO, Tao GZ, Toivola DM, Liao J (2006) “Heads and tails” of intermediate filament phosphorylation: Multiple sites and functional insights. *Trends Biochem Sci* 31:383–394.
- Nixon RA, Sihag RK (1991) Neurofilament phosphorylation: a new look at regulation and function. *Trends Neurosci* 14:501–506.
- Gibb BJ, Brion JP, Brownlee J, Anderton BH, Miller CC (1998) Neuropathological abnormalities in transgenic mice harbouring a phosphorylation mutant neurofilament transgene. *J Neurochem* 70:492–500.
- Rao MV, et al. (2002) Gene replacement in mice reveals that the heavily phosphorylated tail of neurofilament heavy subunit does not affect axonal caliber or the transit of cargoes in slow axonal transport. *J Cell Biol* 158:681–693.
- Rao MV, et al. (2003) The neurofilament middle molecular mass subunit carboxyl-terminal tail domains is essential for the radial growth and cytoskeletal architecture of axons but not for regulating neurofilament transport rate. *J Cell Biol* 163:1021–1031.
- Ackerley S, et al. (2003) Neurofilament heavy chain side arm phosphorylation regulates axonal transport of neurofilaments. *J Cell Biol* 161:489–495.
- García ML, et al. (2003) NF-M is an essential target for the myelin-directed “outside-in” signaling cascade that mediates radial axonal growth. *J Cell Biol* 163:1011–1020.
- Lobsiger CS, García ML, Ward CM, Cleveland DW (2005) Altered axonal architecture by removal of the heavily phosphorylated neurofilament tail domains strongly slows superoxide dismutase 1 mutant-mediated ALS. *Proc Natl Acad Sci USA* 102:10351–10356.
- Goldman JE, Yen SH, Chiu FC, Peress NS (1983) Lewy bodies of Parkinson’s disease contain neurofilament antigens. *Science* 221:1082–1084.
- Rouleau GA, et al. (1996) SOD1 mutation is associated with accumulation of neurofilaments in amyotrophic lateral sclerosis. *Ann Neurol* 39:128–131.
- Lee VM, Otvos L, Jr, Schmidt ML, Trojanowski JQ (1988) Alzheimer disease tangles share immunological similarities with multiphosphorylation repeats in the two large neurofilament proteins. *Proc Natl Acad Sci USA* 85:7384–7388.
- Park SG, Ewalt KL, Kim S (2005) Functional expansion of aminoacyl-tRNA synthetases and their interacting factors: New perspectives on housekeepers. *Trends Biochem Sci* 30:569–574.
- Park SG, et al. (2006) Hormonal activity of AIMP1/p43 for glucose homeostasis. *Proc Natl Acad Sci USA* 103:14913–14918.
- Han JM, et al. (2007) Aminoacyl-tRNA synthetase-interacting multifunctional protein 1/p43 controls endoplasmic reticulum retention of heat shock protein gp96: Its pathological implications in lupus-like autoimmune diseases. *Am J Pathol* 170:2042–2054.
- Ching GY, Liem RK (1993) Assembly of type IV neuronal intermediate filaments in nonneuronal cells in the absence of preexisting cytoplasmic intermediate filaments. *J Cell Biol* 122:1323–1335.
- Heins S, et al. (1993) The rod domain of NF-L determines neurofilament architecture, whereas the end domains specify filament assembly and network formation. *J Cell Biol* 123(Pt 1):1517–1533.
- Sasaki T, et al. (2006) Aggregate formation and phosphorylation of neurofilament-L Pro22 Charcot-Marie-Tooth disease mutants. *Hum Mol Genet* 15:943–952.
- Lee SW, Kim G, Kim S (2008) Aminoacyl-tRNA synthetase-interacting multi-functional protein 1/p43: An emerging therapeutic protein working at systems level. *Expert Opin Drug Discov* 3:945–957.
- Herrmann H, Aebi U (2000) Intermediate filaments and their associates: Multi-talented structural elements specifying cytoarchitecture and cytodynamics. *Curr Opin Cell Biol* 12:79–90.
- Zhu Q, Couillard-Despres S, Julien JP (1997) Delayed maturation of regenerating myelinated axons in mice lacking neurofilaments. *Exp Neurol* 148:299–316.
- Nguyen MD, et al. (2004) A NUDEL-dependent mechanism of neurofilament assembly regulates the integrity of CNS neurons. *Nat Cell Biol* 6:595–608.
- Antonellis A, et al. (2003) Glycyl tRNA synthetase mutations in Charcot-Marie-Tooth disease type 2D and distal spinal muscular atrophy type V. *Am J Hum Genet* 72:1293–1299.
- Jordanova A, et al. (2006) Disrupted function and axonal distribution of mutant tyrosyl-tRNA synthetase in dominant intermediate Charcot-Marie-Tooth neuropathy. *Nat Genet* 38:197–202.
- Nangle LA, Zhang W, Xie W, Yang XL, Schimmel P (2007) Charcot-Marie-Tooth disease-associated mutant tRNA synthetases linked to altered dimer interface and neurite distribution defect. *Proc Natl Acad Sci USA* 104:11239–11244.
- Seburn KL, Nangle LA, Cox GA, Schimmel P, Burgess RW (2006) An active dominant mutation of glycyl-tRNA synthetase causes neuropathy in a Charcot-Marie-Tooth 2D mouse model. *Neuron* 51:715–726.
- Mersyanova IV, et al. (2000) A new variant of Charcot-Marie-Tooth disease type 2 is probably the result of a mutation in the neurofilament-light gene. *Am J Hum Genet* 67:37–46.
- Knies UE, et al. (1998) Regulation of endothelial monocyte-activating polypeptide II release by apoptosis. *Proc Natl Acad Sci USA* 95:12322–12327.
- Wang Y, et al. (2006) Association of beta-arrestin and TRAF6 negatively regulates Toll-like receptor-interleukin 1 receptor signaling. *Nat Immunol* 7:139–147.
- Athlan ES, Mushynski WE (1997) Heterodimeric associations between neuronal intermediate filament proteins. *J Biol Chem* 272:31073–31078.
- Fitzsimonds RM, Song HJ, Poo MM (1997) Propagation of activity-dependent synaptic depression in simple neural networks. *Nature* 388:439–448.
- Xu L, et al. (2005) Cystatin C prevents degeneration of rat nigral dopaminergic neurons: In vitro and in vivo studies. *Neurobiol Dis* 18:152–165.